JOURNAL OF MATERIALS SCIENCE **39** (2004) 4119–4129

Behavior of solid lubricant nanoparticles under compression

V. LESHCHINSKY
Holon Institute of Technology, Holon 58102, Israel

R. POPOVITZ-BIRO, K. GARTSMAN, R. ROSENTSVEIG
Weizmann Institute of Science, Rehovot, Israel

YU. ROSENBERG
Wolfson Applied Materials Research Center, Tel-Aviv University, Tel-Aviv, Israel

R. TENNE
Weizmann Institute of Science, Rehovot, Israel

L. RAPOPORT*
Holon Institute of Technology, Holon 58102, Israel
E-mail: rapoport@hait.ac.il

Inorganic fullerene-like materials have been identified as being of potentially utmost importance for many industrial applications. MoS_2 and WS_2 hollow nanoparticles have been identified as strong candidates for tribological applications such as solid lubricants. The main goal of this work was to evaluate the mechanical properties of solid lubricant particles in ensemble under hydrostatic pressure. The behavior of nanopowders under compression has been described on the basis of constitutive models of continuum mechanics. The model will be applied to an isotropic compaction of copper (well-studied medium), fullerene-like (IF-WS_2) nanoparticles and a natural powder of 2H-WS_2 platelets. The morphology of individual nanoparticles and nanoparticle ensembles will be examined and discussed. Another aspect of this work was to study the applicability and limitations of the proposed constitutive model for the understanding of the tribological behavior of solid lubricant nanoparticles. Compression with the maximal pressure (500 MPa) showed that the shape of the IF nanoparticles is preserved. The dominant mechanism of damage was found to be the delamination or peeling-off of the external sheets of hollow nanoparticles. Strong destruction of 2H-WS_2 platelets was observed under compression.

1. Introduction

Inorganic fullerene-like materials have been identified as being of potentially utmost importance for many industrial applications, as a consequence of their unique mechanical and electronic properties. In analogy to carbon fullerenes (C_{60}, etc.), fullerene-like materials are made of two-dimensional lamellar structure, like BN, CN_x, MoS_2, $CdCl_2$, etc., with closed and curved morphologies, grown into three-dimensional networks or architectures and displaying a wide range of shapes. As a consequence of their atomic-scale structure involving strong covalent bonds and noncompact space filling, these materials have been identified as strong candidates for tribological applications such as solid lubricants [1]. Detailed analysis of the nanoparticles properties is essential to gain understanding of the complex physical behavior of this nanopowder at the interface during a friction test. There are some works attempting to characterize individual fullerene-like nanoparticles (see for example [2, 3]). However evaluation of the nanoparticle behavior in ensemble as a medium has not yet been studied. Thus the main goal of this work was to evaluate the mechanical properties of solid lubricant particles in ensemble. As a first step, hydrostatic compression of the solid lubricant nanoparticles which provides uniform loading of a particulate media has been studied. In a forthcoming work the properties of a solid lubricant medium under compression with a shear will be considered.

2. Background

2.1. The phenomenological model of nanoparticle media

It is well established that a densification of the particulate media occurs in the following succession [4]:

*Author to whom all correspondence should be addressed.

(i) rearrangement of grains (particles), (ii) fracture and rearrangement of grains and (iii) deformation and fracture of grains. At the first stage of densification of a loose powder the particle rearrangement is obtained by an interparticle sliding which depends on the friction properties of nanoparticles. The cohesion between the powder particles increases with the relative density. If the cohesion is very high, the powder system behaves like a sintered porous material (third mechanism) [5]. The deformation and fracture of particles are defined by their bulk properties. Thus the main task of the powder compression analysis is to evaluate both the friction properties of the solid lubricant medium and the bulk properties of particles. In general, the compression of a powder is characterized by compaction curve (pressure-density relationship). The behavior of powders under compression has been described on the basis of constitutive models of continuum mechanics [4–12]. Many of these models were originally developed for the sintered powders. However, the loose powder behaves differently from the sintered ones. Many of the differences between a powder media and porous body originate from the individuality of the powder particles in a powder system. In addition to particles distortion (plastic deformation for metal powders), fragmentation (for ceramic and pharmaceutical powders) or crystallographic glide (for oxide aggregates), the assemblage of powder particles can move and rotate against each other with interfacial friction or cohesion.

The continuum models determine the yield condition of porous medium using second deviator stress invariant J_2' and first stress invariant J_1. One general form of the yield function proposed in many works (for example, [6]):

$$\phi = AJ_2' + B(J_1 + k)^2 - Y^2 = 0 \tag{1}$$

where A, B and k are functions of the relative density ρ, and Y is the apparent flow stress which is at least a function of the relative density. Also

$$J_1 = \sigma_{kk} = 3\sigma_m, \quad J_2' = \frac{1}{2}\sigma_{ij}'\sigma_{ij}', \qquad \sigma_{ij}' = \sigma_{ij} - \sigma_m\delta_{ij} \tag{2}$$

where: σ_m is the mean stress, σ_{ij} is the macroscopic stress, δ_{ij} is the Kronecker delta function.

The various models for porous metals as reviewed in Refs. [13, 14] are all in the form of Equation 1 with $k = 0$. The physical reason for including the coefficient k in Equation 1 is to reflect the limited inter-particle strength when it is subjected to a tensile stress state. In order to use Equation 1 for porous materials and different powders alike, it was assumed that the apparent flow stress Y is a fraction of the flow stress for the individual particle, Y_0, i.e.

$$Y^2 = \eta(\rho)Y_0^2 \tag{3}$$

One can see from (3), that the parameter $\eta(\rho)$ depends only on the relative density of the porous material and represents the square of the Y/Y_0 ratio. The specific forms of A, B, k and η in Equation 1 relies greatly upon the experimental and material data. The hydrostatic pressing of powder and green strength of powder compact have been used in order to determine the coefficients A, B and k [6]. However, the above relations have not been rigorously proved for loose powders.

In the present work, the phenomenological model based on Equation 1 will be used in order to describe the constitutive behavior of nanoparticle media during a general isotropic compression. The shape of the powder particles is an important characteristic at the first stage of compression where sliding and the local plastic deformation play an important role [5]. The model will be applied to an isotropic compaction of copper (well-studied medium), fullerene-like (IF-WS_2) nanoparticles and a natural powder of 2H-WS_2 platelets, having very different particle morphology. This new constitutive model takes into account the combined influence of particles morphology, agglomeration and distortion of the solid lubricant medium on the behavior of the powder under compression. Another aspect of this work was to study the applicability and limitations of the proposed constitutive model for the understanding of the tribological behavior of solid lubricant nanoparticles. Additionally the morphology of individual nanoparticles and nanoparticle ensembles will be examined and discussed.

2.2. Yield function and properties estimation

We propose to use the yield function of Equation 1, with a new approach to determine the flow stress of individual particles, Y_0 and a function of the particle ensemble, k, as the main mechanical characteristics of a powder body. First, we consider an isotropic (hydrostatic) compression. In this case the yield function (1) is transformed into:

$$B(J_1 + k)^2 - Y^2 = 0 \tag{4}$$

According Tszeng and Wu [6], the function-k is zero when an inter-particle sliding during compression is stopped and the material becomes porous and consolidated. In the case, when the densification of this material is associated with a plastic deformation, the flow stress of individual particles, Y_0 can be calculated. The coefficients A, B and η are assumed to be functions of the density [6]:

$$A(\rho) = 2 + \rho^2; \quad B(\rho) = \frac{1-\rho^2}{3}; \qquad \eta(\rho) = \frac{\rho^2 - \rho_c^2}{1 - \rho_c^2} \tag{5}$$

where ρ_c is the critical relative density, where the yield stress of the powder is zero. Thereafter, Equations 3 and 4 with the porosity functions (5) serve to fulfill the definition of the flow stress during an isotropic compression of the powder at high density. Inserting (5) into (4) and taking into account that $k = 0$, the flow

stress of individual particles can be expressed as:

$$Y_0^2 = \frac{3(1-\rho^2)\left(1-\rho_c^2\right)}{\rho^2-\rho_c^2}\,p^2 \qquad (6)$$

Therefore, the k-function in Equation 4 is given by:

$$\kappa = Y_0\left[\frac{3\left(\rho^2-\rho_c^2\right)}{(1-\rho^2)\left(1-\rho_c^2\right)}\right]^{\frac{1}{2}} - 3p \qquad (7)$$

3. Experimental procedure

The experiments were conducted using fullerene-like nanoparticles (IF-WS_2), commercially available layered 2H-WS_2 particles and water-atomized copper powder. Details of the IF synthesis are presented in Ref. [3]. The characteristics of the studied particles are given in Table I. The average size of the IF-WS_2 particles was close to 120 nm, Fig. 1a, while it was 4 μm for 2H-WS_2, (Fig. 1b).

Atomized copper powders show more or less round shape. The IF-WS_2 nanoparticles have either ovoid,

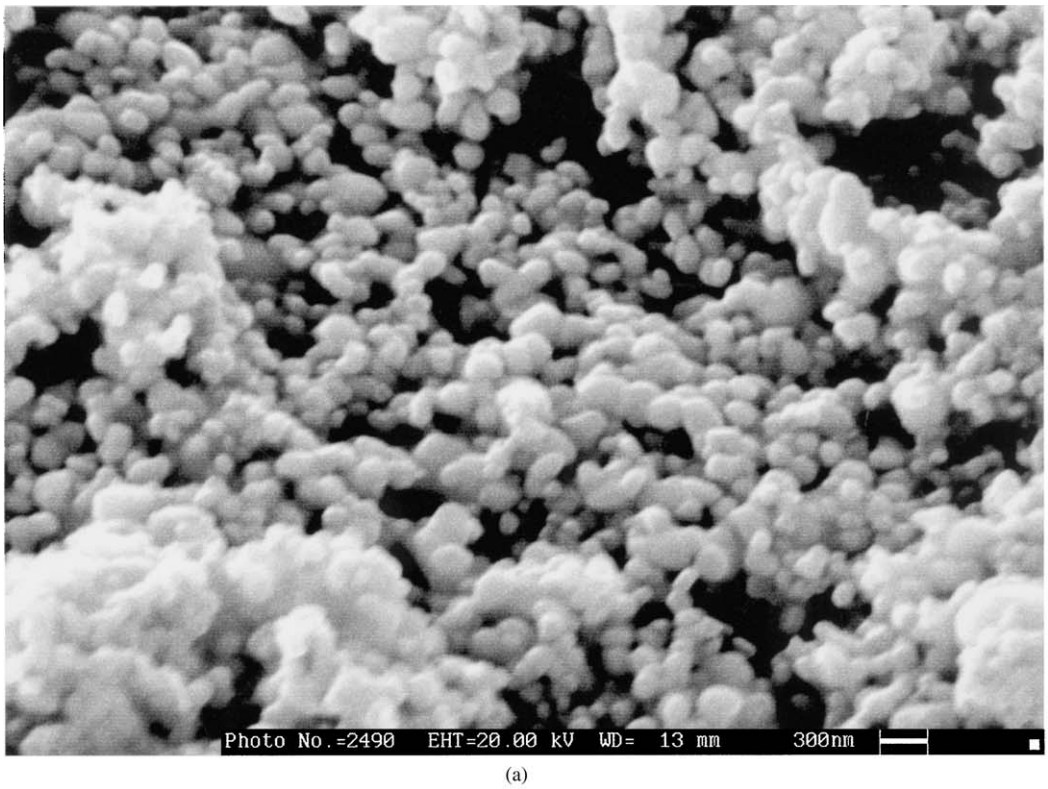

(a)

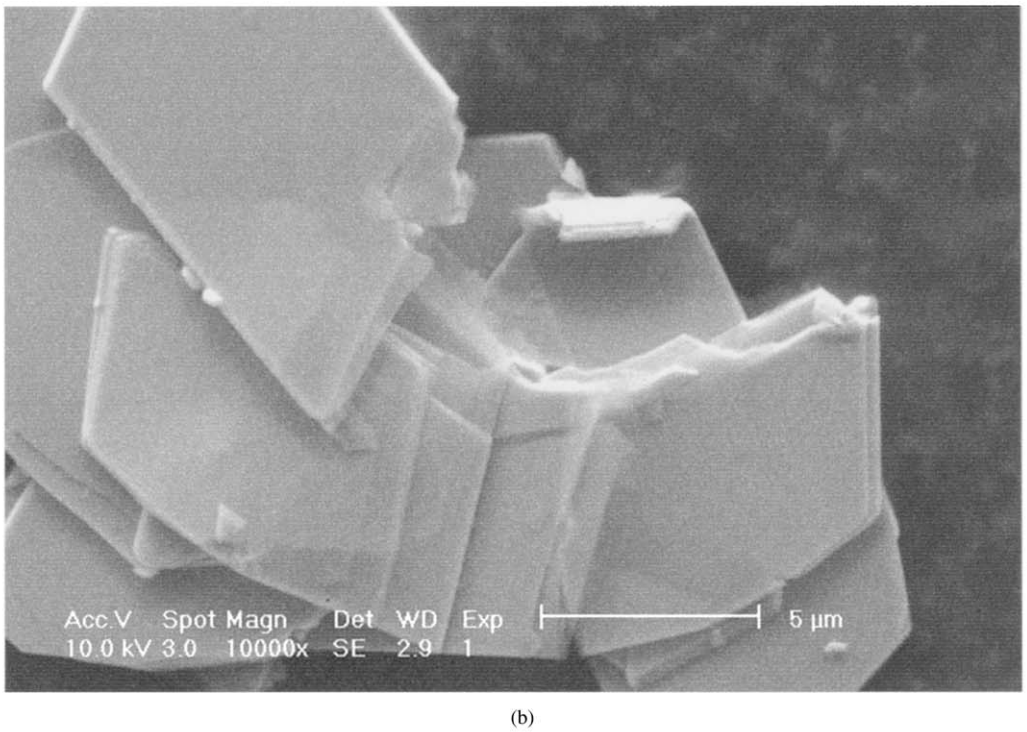

(b)

Figure 1 Fullerene-like IF-WS_2 nanoparticles (a) and layered commercially available platelets of WS_2 (b).

TABLE I Characteristics of IF-WS_2, 2H-WS_2 and copper powders

	IF-WS_2 nanopowder	2H-WS_2 powder	Water-atomized copper powder
Apparent relative density	0.197	0.208	0.395
Tap relative density	0.278	0.293	0.449
Particle size distribution* (μm)	–	–	
−140			1.4
−140 to +200			23.3
−200 to +325			75.3
−325			

*US standard sieve (wt%).

quasi-spherical shape whilst 2H-WS_2 come in platelet morphology.

The hydrostatic powder compression experiments were carried out using quasi-hydrostatic polyurethane bag tooling. The hydrostatic pressure was changed in the range of 3–500 MPa. After cold hydrostatic pressing (**CHP**), the density of the green compact was measured by Archimedes' method. The **CHP** was performed using INSTRON test machine with a load capacity of 200KN. The load-displacement diagrams were computer recorded and they were corrected to take into account the deformation of the polyurethane bag. The density of the green compact measured after densification was used in the analysis of the pressure-density curve. The deformation and fracture of IF and 2H particles were analyzed using Transmission electron microscope (TEM)- Philips model CM120 (120 kV); high resolution scanning electron microscope (HRSEM) FEI model XL-30 equipped with a field emission gun, and X-ray diffraction. Specimens for TEM examination were prepared by touching the compressed pellet of nanoparticles with a carbon/collodion coated copper TEM grid. XRD patterns were collected in the range 2–90° (2Θ) with CuK_α radiation on the Θ-Θ powder diffractometer "Scintag X_1" equipped with a liquid nitrogen cooled Ge solid-state detector. Peak positions and widths of the Bragg reflections were determined by a self-consistent profile-fitting procedure using the Pearson VII function [15]. Lattice constants computation was carried out by a reciprocal lattice parameter refinement; microstrains in radial direction were estimated by Williamson—Hall approach [16] from (0.02 L) (L = 1 ÷ 4) peaks broadening.

4. Results

4.1. Pressure-density relation

Fig. 2 shows the relationships between the hydrostatic pressure and density for three powdered compacts. The density of 2H-WS_2 powder compact under maximal pressure, $p = 500$ MPa, is seen to be (6 g/cc), while it was 5.37 g/cc for IF-WS_2 (Fig. 2a). The theoretical density of a natural 2H-WS_2 is known to be 7.2 g/cc [17]. The calculated density of IF-WS_2 was 6.6 g/cc [1]. The difference in the densities between the observed and calculated values is associated with the hollow cage structure of the IF nanoparticles [1]. As seen from Fig. 2, two ranges of the density variation are observed with pressure increasing-quick and slow change in the density for low and high values of the pressure. The relative densities of the powder media were different for each type of powder at the low pressure range. The compressibility of IF-WS_2 nanoparticles is much larger than that of both 2H-WS_2 and copper powders at the first stage of compression.

At higher hydrostatic pressures a saturation value of the density was obtained at a pressure close to 300 MPa. For the 2H-WS_2 powder, a tendency for slower increase in the density was observed under high pressure. It is expected that the character of densification is typical for each of the above powders and depends on the initial structure of the particles and the mechanisms of compression. The structural characteristics of IF and 2H particles at the different stages of compression will be considered below.

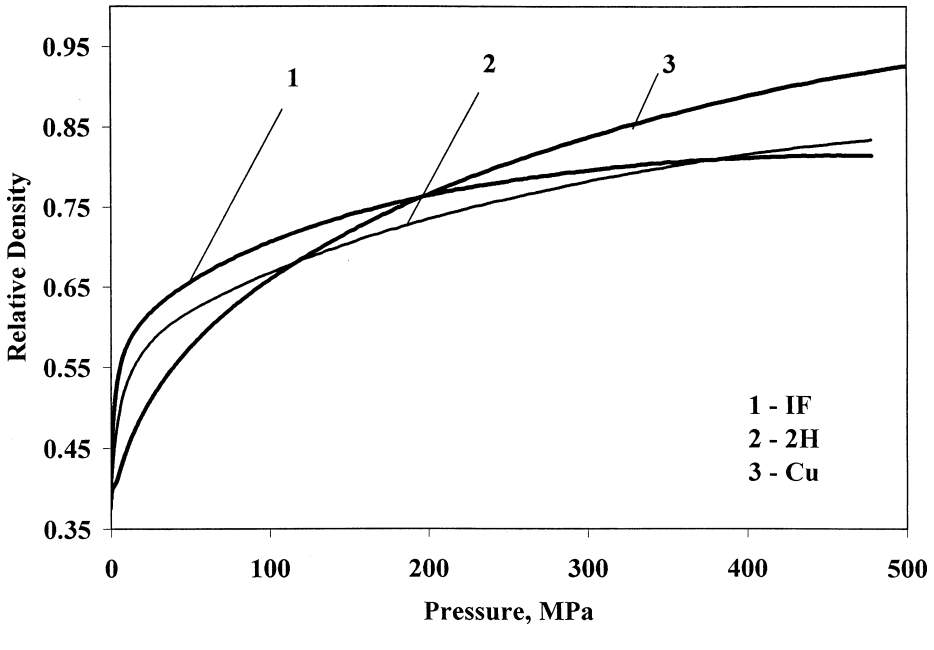

Figure 2 The relationships between the hydrostatic pressure and relative density for three powdered compacts: IF, 2H and Cu powders.

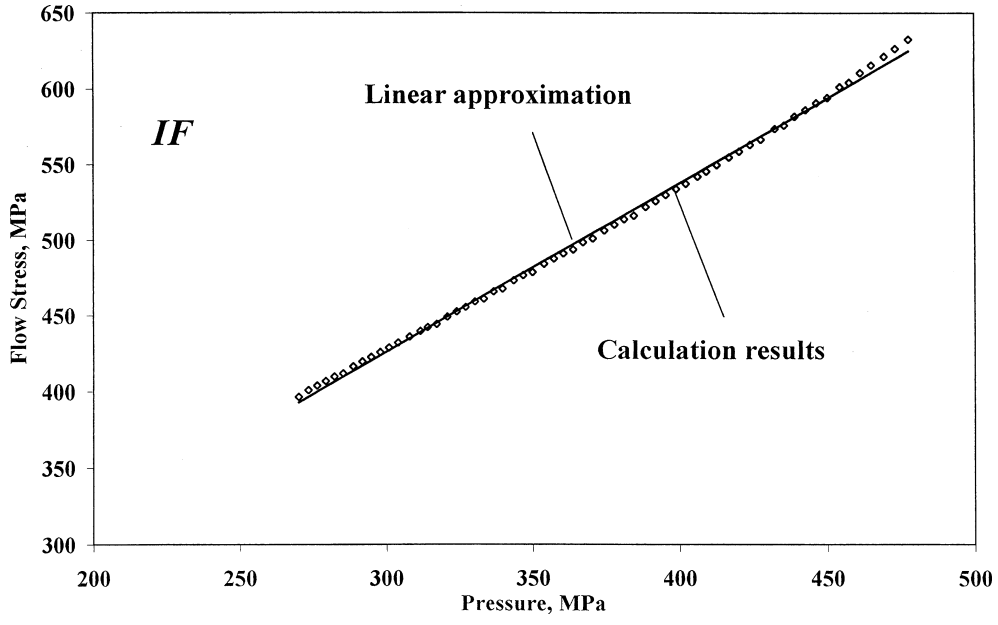

Figure 3 Flow stress-pressure relationships for IF (a) and 2H (b) media.

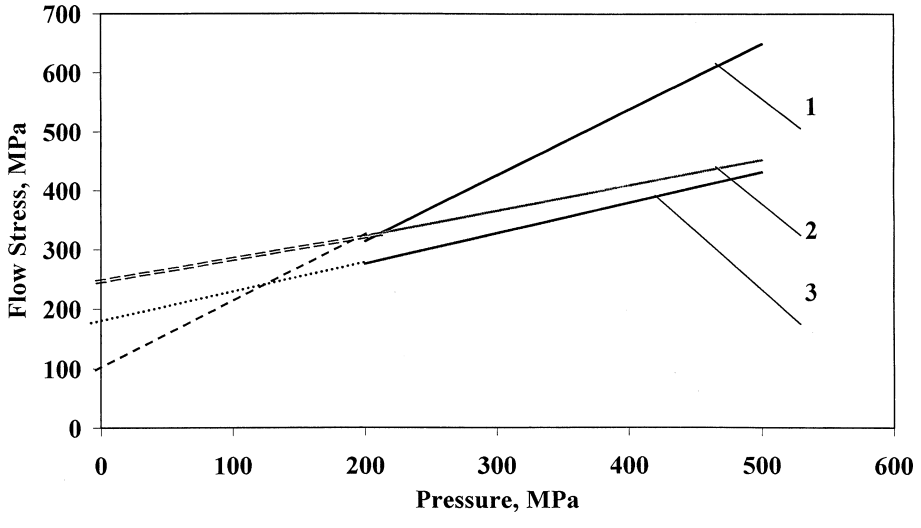

Figure 4 The linear approximations of flow stress-pressure curves for IF (1), 2H (2) and Cu (3) media.

4.2. Grains' flow stress determination

The results of the flow stress determination are shown in Figs 3 and 4. To determine the flow stress, relationship (6) was used. A permanent increase of the flow stress due to hardening of the powder during compression of the powder ensemble is observed. The initial flow stress of individual particles was calculated using linear approximation of flow-stress-hydrostatic pressure curves. One can see (Figs 3 and 4) that a part of the pressure-density curve at the high density range can be approximated as a linear curve for all the materials studied with sufficiently high reliability. The equations for these approximations are shown in Table II.

4.3. Approximation for the flow stress-pressure curves

These data reveal that the flow stress—compression stress dependence may be represented as $Y_0 = \lambda p + Y_S$, where Y_S is an initial flow stress of the base solid (bulk) material at a hydrostatic pressure $p = 0$, λ— is a hardening coefficient. It should be noted that for metal powders the initial flow stress is equivalent to the yield strength of the bulk metal. Actually the initial flow stress of copper estimated in the present study is slightly higher than the documented yield strength of the bulk metal determined by classical tensile test. This discrepancy may be attributed to differences between the mechanical properties of metal powder and bulk metal due to different metallurgical history of the tested materials and oxidation of the coper surface [5]. A comparison

TABLE II Approximation equations for powders

Powder	Equation	R^2
WS_2IF	$Y_0 = 1.1159P + 91.442$	$R^2 = 0.9983$
$WS_2$2H	$Y_0 = 0.5208P + 171.63$	$R^2 = 0.9992$
Cu	$Y_0 = 0.4352P + 234.87$	$R^2 = 0.992$

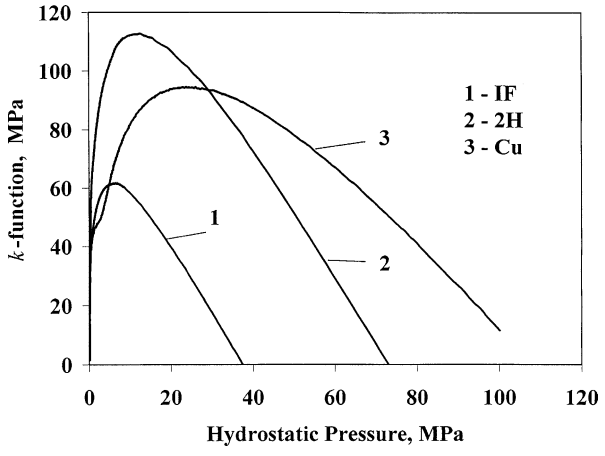

Figure 5 k-function for IF, 2H and Cu media in low pressure range.

of the initial flow stress Y_S of the fullerene-like nanoparticles with 2H-WS_2 platelets and copper particles show that Y_S of the IF-WS_2 is minimal while the hardening coefficient is maximal for this powder. The hardening of the IF-WS_2 nanoparticles is so high that the compressibility of this nanoparticle medium at the final stages of powder compression is lower than that of the other powders (Fig. 2).

4.4. Interparticle strength function, κ

The κ—function has been calculated in the range of low hydrostatic pressures using the Equations 1 and 7. The results of this calculation are summarized in Fig. 5. The real values of κ have a positive sign and tend to zero as the pressure increases. One can see that the interparticle

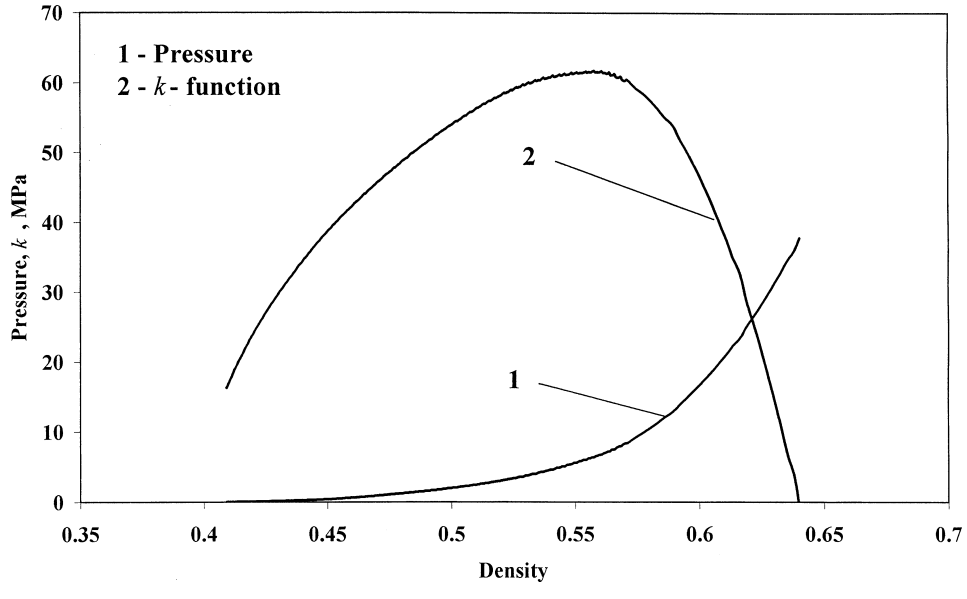

Figure 6 The connection between k—function, hydrostatic pressure and density in low dense zone for IF nanoparticles media.

Figure 7 The virgin structure of hollow and closed IF-WS_2 nanoparticles.

strength of IF-WS_2 nanoparticles is smaller by a factor of two compared to that of 2H-WS_2. In other words, IF-WS_2 nanoparticle media shows the best slippery nature in comparison to 2H and copper powder at the low pressure range. The rearrangement of grains (particles) occurs up to densities 0.60–0.65 and in these range of densities the interparticle strength is strongly influenced by grain sliding (Fig. 6).

4.5. The effect of compression on the structure of IF and 2H particles

In order to analyze the change of the shape and the structure of the IF and 2H solid lubricant particles as a medium under compression, their virgin state has been originally studied using TEM and HRSEM microscopy. The virgin shape of the hollow and closed IF nanoparticles was found to be ovoid and irregular (see Fig. 7). Tilting of the IF-WS_2 samples in the TEM showed that the lattice images of the IF-WS_2 nanoparticles remain essentially unchanged, attesting the closed nature of the nanoparticles (see Fig. 8). The average size of the IF-WS_2 nanoparticles was found to be close to 120 nm. The compression with maximal pressure showed that the shape of the IF nanoparticles is apparently preserved (see Fig. 9). The dominant mechanism of damage was found to be the exfoliation or pilling off the external sheets of the hollow nanoparticles. It is important to note that although the external sheets of IF-WS_2 nanoparticles were peeled-off, the shape of the nanoparticles after distortion remained essentially unchanged compared with the virgin state. A typical ensemble of single and agglomerated IF-WS_2 solid lubricant nanoparticles after compression is shown in Fig. 10. It is expected that the mobility of such "spherical" nanoparticles can be high in comparison to 2H and Cu powders at the first stage of compression where the structure of the powder is preserved and the nanoparticles are free to slip and rotate. Free-spread 2H-WS_2 particles with platelet morphology are shown in Fig. 11. Appreciable destruction occurred for the compressed 2H-WS_2 platelets (see Fig. 12).

X-Ray analysis (XRD) of the IF-WS_2 medium showed that cell parameters of most compressed

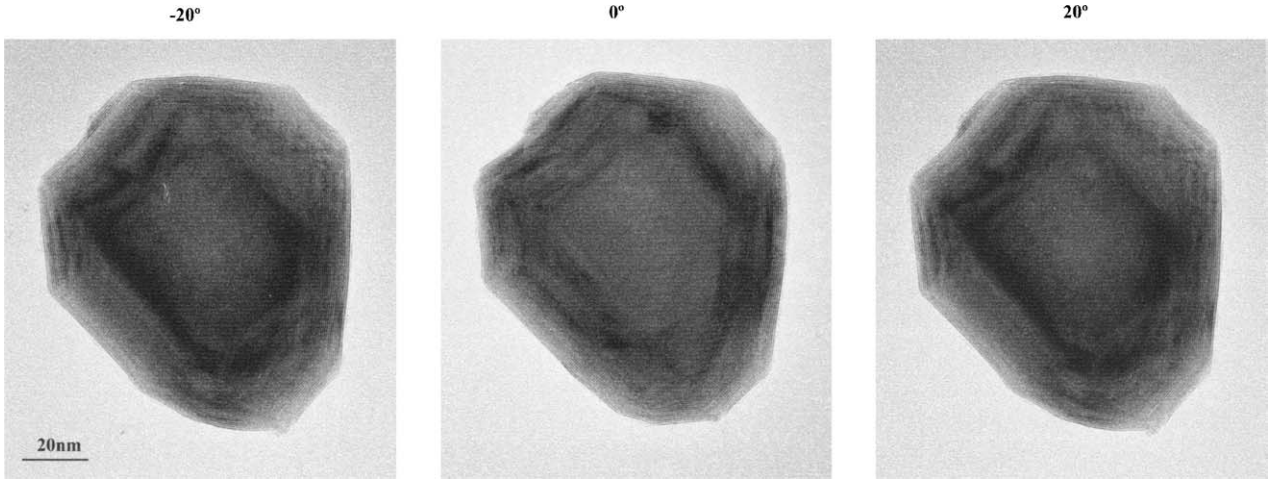

Figure 8 The tilting of the IF-WS_2 nanoparticles in the virgin state confirms the preservation of their form in different directions.

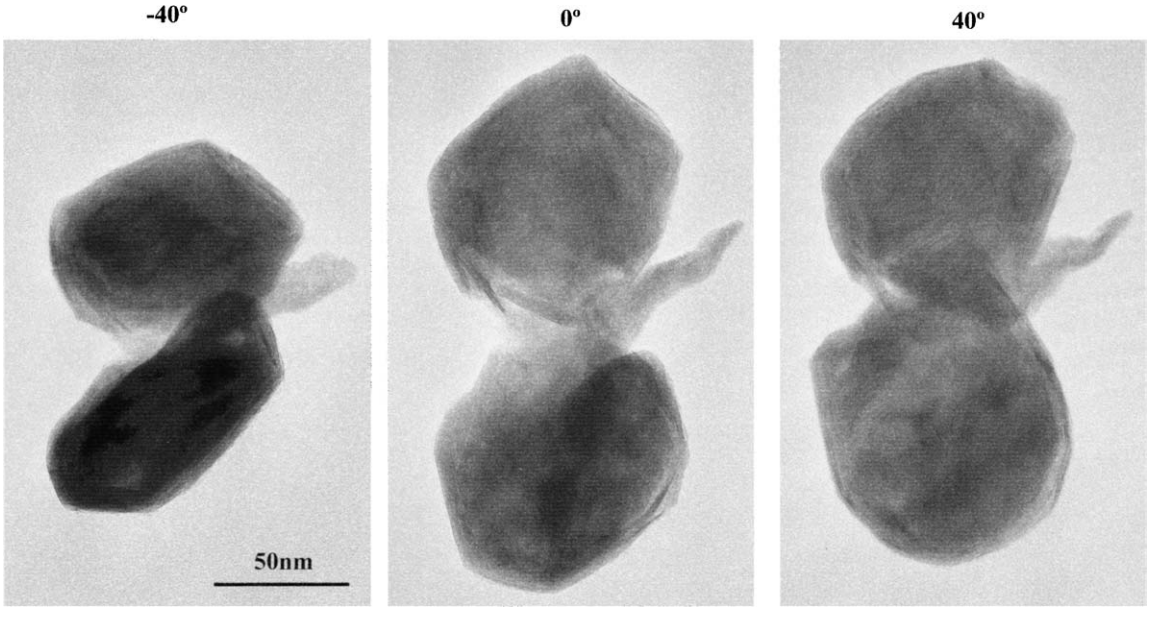

Figure 9 The tilting of the IF-WS_2 nanoparticles after high pressure compression ($P = 500$ MPa).

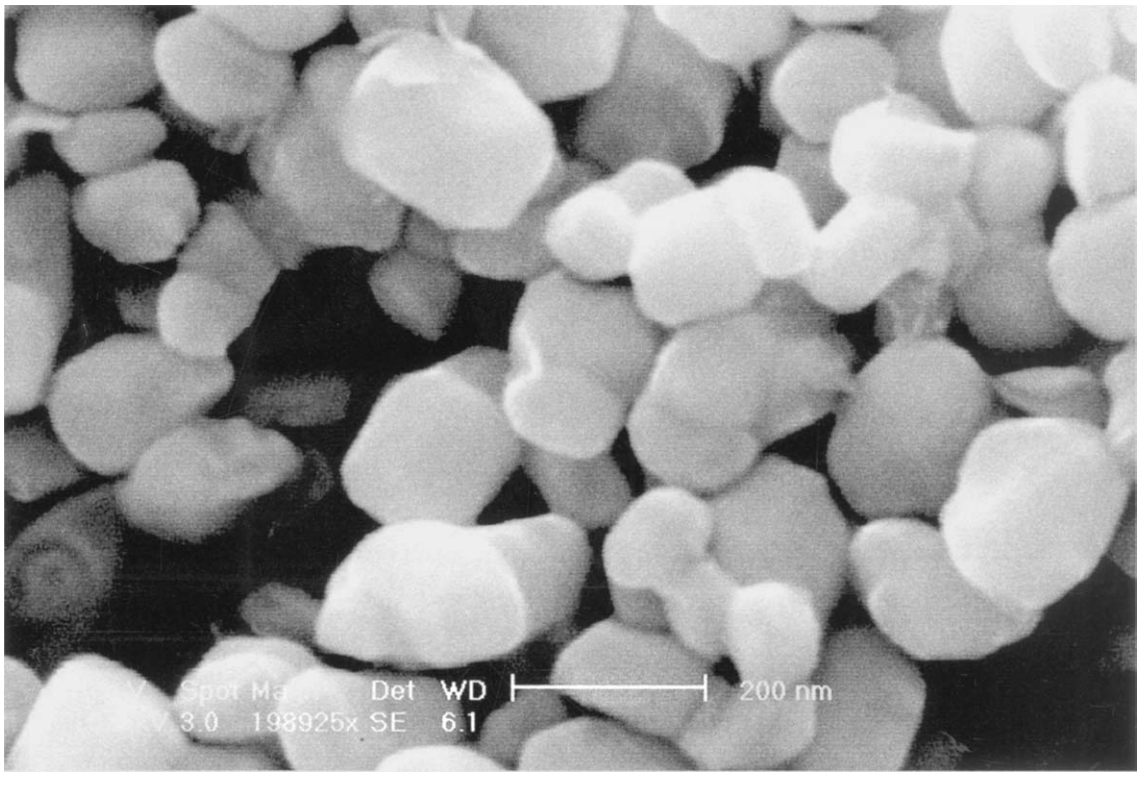

Figure 10 The ensemble of IF-WS_2 solid lubricant nanoparticles after compression.

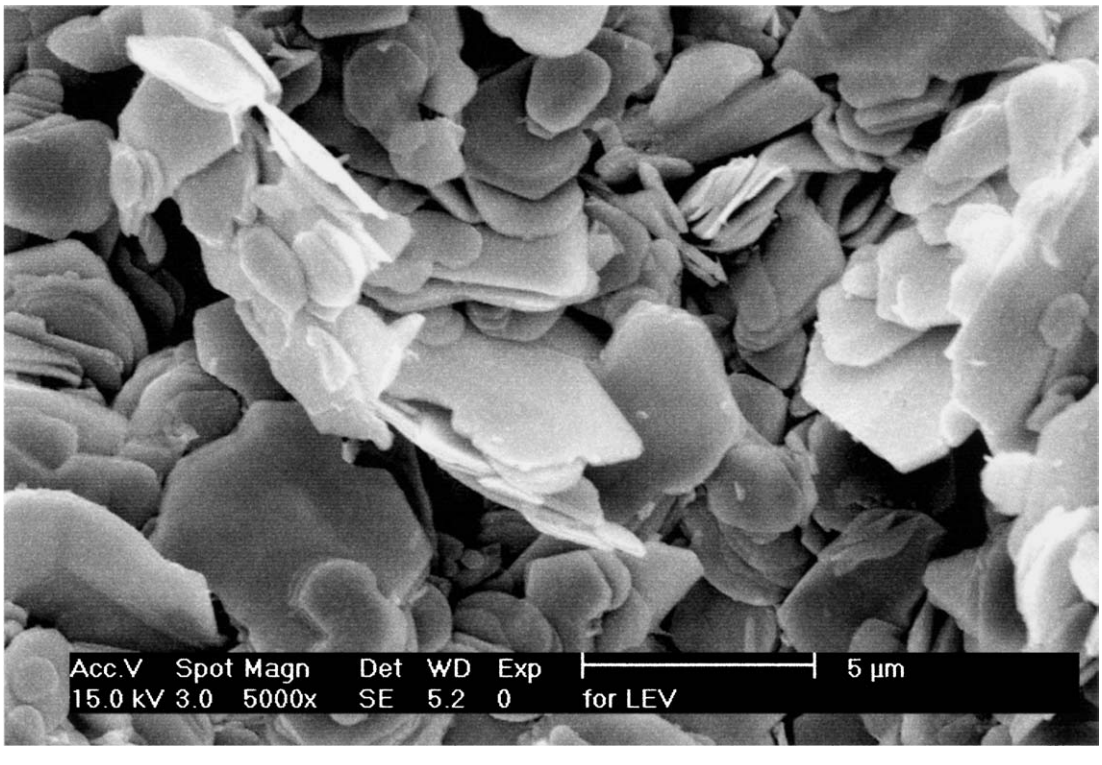

Figure 11 Free-spread layered 2H-WS_2.

IF-WS_2 particles $A = 3.153 \pm 0.001$ Å and $C = 12.497 \pm 0.005$ are very close to the original ones $A = 3.154 \pm 0.001$ Å and $C = 12.512 \pm 0.005$ Å. Compression has no effect on the microstrains in the radial direction: $\langle \Delta C/C \rangle = (10.83 \pm 0.45) \cdot 10^{-3}$ for most compressed vs. $(11.19 \pm 0.62) \cdot 10^{-3}$ for the original media. Having in mind also that the size of coherent scattering domains ($\approx$ IF shell thickness) in both cases is beyond a high bound detectable by Bragg reflections broadening, we may conclude that the XRD results confirm the results of the TEM and SEM study: the bulk structure of the IF-WS_2 medium under compression with pressure of 500 MPa does not change. Thus the X-Ray analysis of the IF medium after compression confirmed the data of TEM and SEM study. Therefore it may be concluded that these nanoparticles are capable

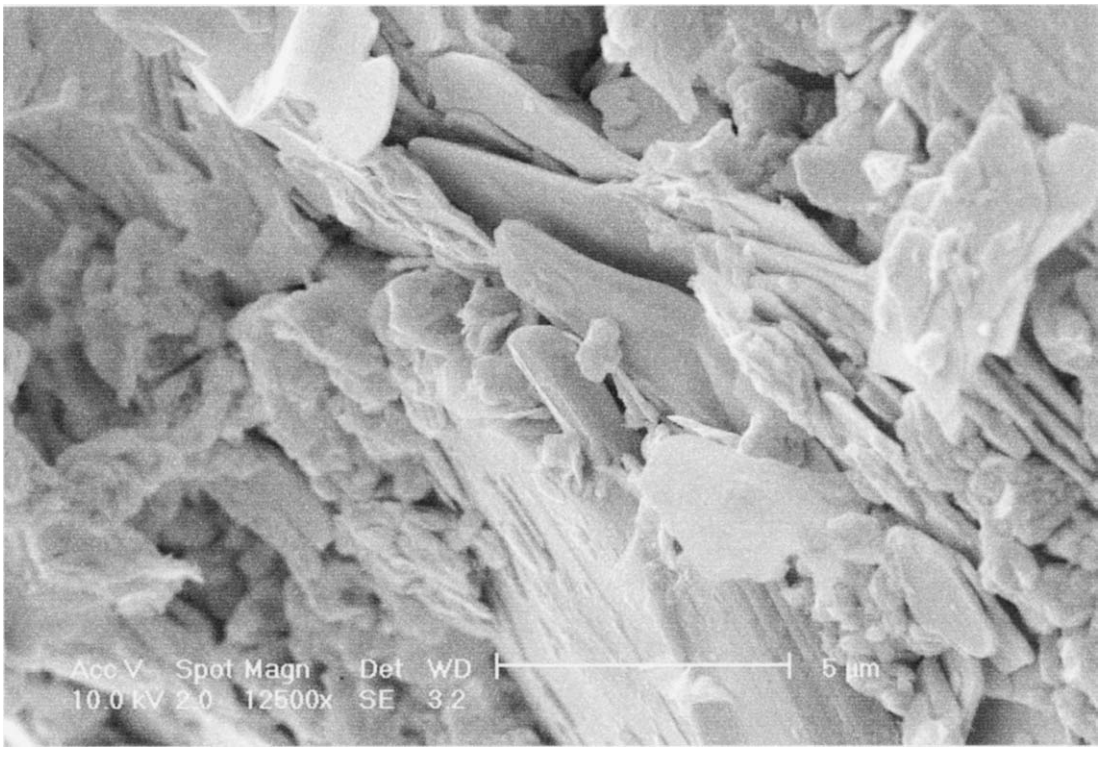

Figure 12 Strong destruction of 2H-WS_2 platelets after compression.

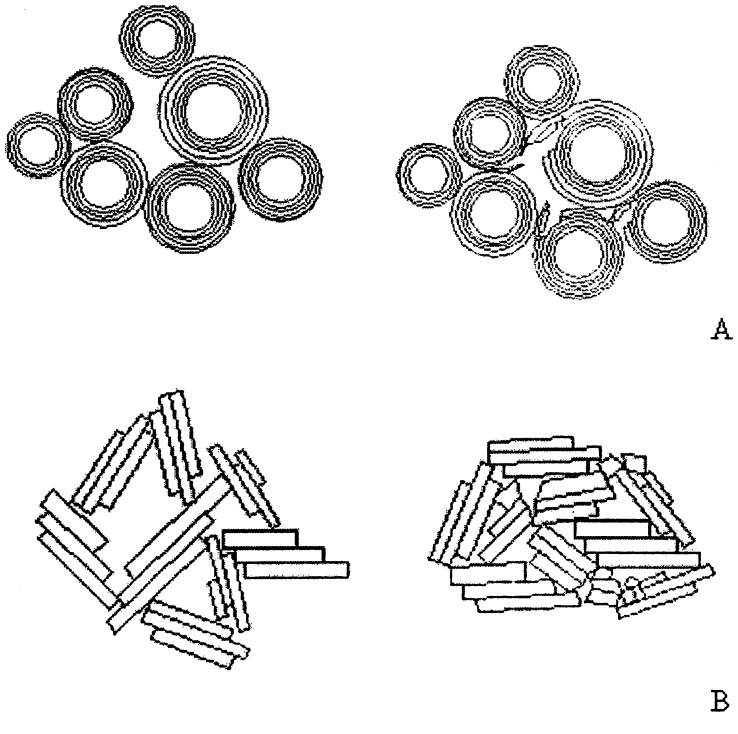

Figure 13 The scheme of compression of IF (A) and 2H (B) solid lubricant particles in the ensemble.

of withstanding a high hydrostatic pressure, caused by the compression stress. Mainly, only the outermost layers of the IF-WS_2 medium are damaged, which affect on the tribological behavior of this material.

5. Discussion

5.1. The behavior of solid lubricant particles under hydrostatic compression

Compression of soil or ceramic powders can be attributed to a number of mechanisms: (i) rearrangement of the grains, (ii) fracture and rearrangement of the grains, (iii) distortion or deformation (for example, bending) of the grains [4]. It is expected that mainly the first two mechanisms of compression can occur for the IF-WS_2 hollow cage nanoparticles while the 2H-WS_2 particles may be also distorted and bended due to their platelet shape. The behavior of the solid lubricant particles at the low-pressure range is determined mainly by the slippery nature of the particles. The IF-WS_2 initial flow stress is found to be lesser than those of 2H-WS_2 and the copper powder. This effect usually

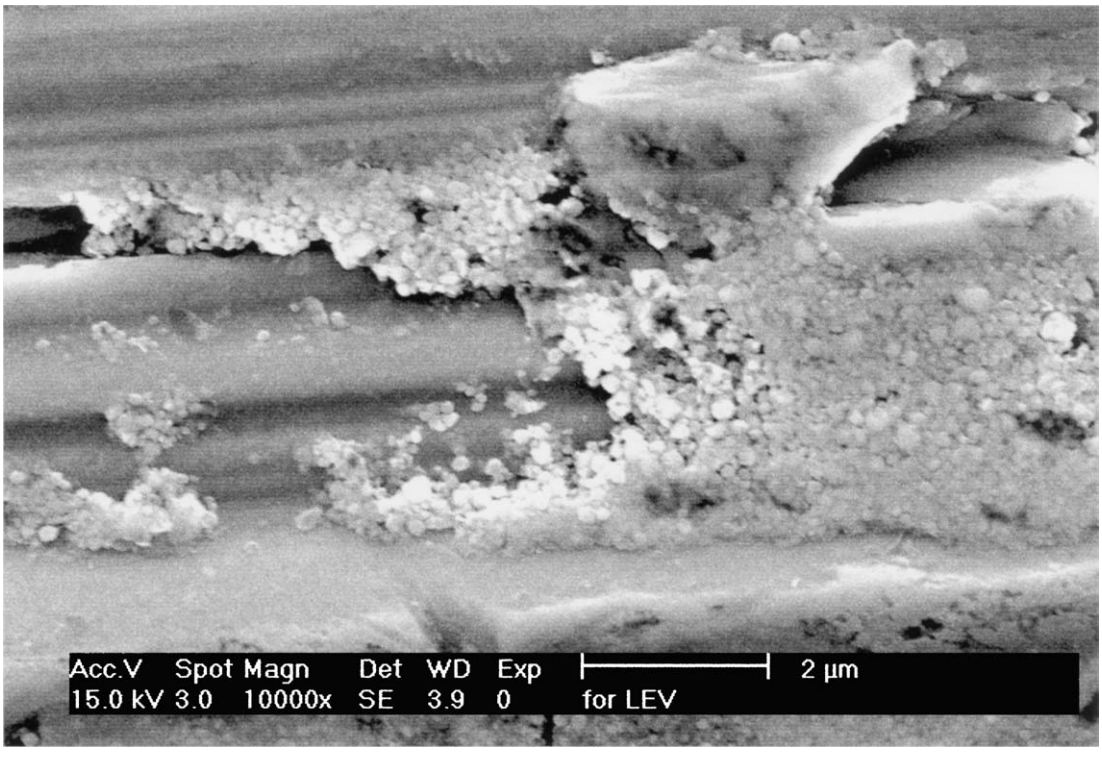

Figure 14 IF-WS_2 nanoparticles in the valleys of rubbed surfaces.

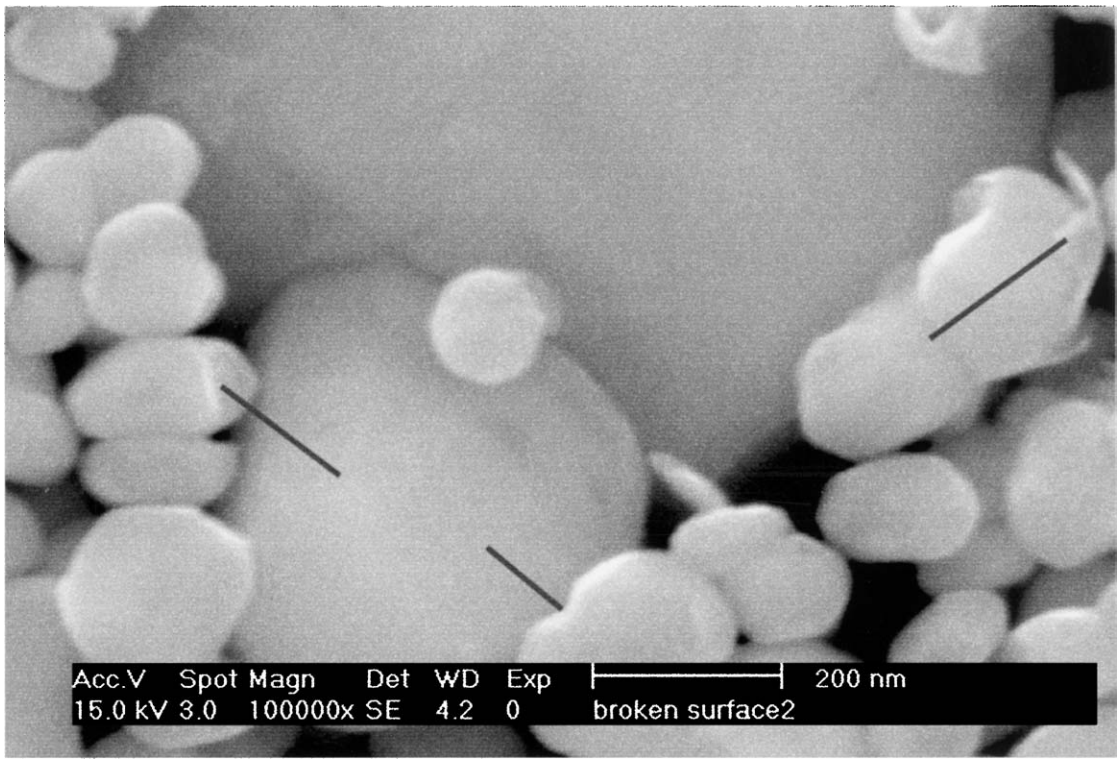

Figure 15 The damage and exfoliation of external sheets of IF nanoparticles after the friction (noted by arrows).

provide easy slipping of IF nanoparticles in the ensemble when low pressure is applied. Thus it may be concluded that the IF-WS_2 nanoparticle media shows the best slippery nature in comparison to 2H and copper powder at the range of low pressure compression. This behavior may be attributed to the close, ovoid shape of the IF allowing easy intergranular friction under low hydrostatic pressure. No effective sliding is obtained under compression in the area of high density compact. Two mechanisms of particles compression characterize this range-rearrangement of the particles and their deformation and/or distortion. These mechanisms can not be easily distinguished and the transition from one mechanism to the other can not be easily recognized. It was found that the strength of the IF-WS_2 nanoparticles is much larger than that of the 2H-WS_2 at the high pressure range. The exfoliation of only the external layers of the IF nanoparticles, preservation of their

shape and their lattice parameter as confirmed by SEM, TEM and X-Ray allude to the very high stiffness of fullerene-like nanoparticles. At the same time a second range of the compression under high pressure is characterized by local delamination of the external sheets of the IF nanoparticles. The damage of IF-WS_2 nanoparticles is believed to occur by the gradual peeling off of these external thin sheets (see Fig. 9). Contrarily, the platelet particles exhibit heavy damage under high pressure loading. They are being bended and distorted due to the local interparticle stresses acting in the powder media at high pressure. For this reason the compressibility of the 2H-WS_2 platelet particles is higher than that of IF-WS_2 nanoparticles at high hydrostatic pressures. The principal scheme of the particle compression based on the analysis of their behavior, is shown in Fig. 13.

5.2. The behavior of solid lubricant particles under friction

The results obtained in this work allow to understand better the friction and wear behavior of IF-WS_2 nanoparticles in the interface between rubbed surfaces [1, 20]. It is interesting to note that the first change of the shape of the IF-WS_2 nanoparticles under friction was observed in the range close to 300 MPa [21] in the transition from low to high pressure compression. The high stiffness of the IF nanoparticles which is revealed in the present work allows apparently to explain the increase of the number of ploughing tracks on the surface of soft sample lubricated with oil + IF nanoparticles in comparison to friction with a pure oil [22]. It was shown that the IF nanoparticles are stored in the valleys of the contact surfaces (see Fig. 14). It may be seen that the damage development under friction occurs in a similar manner to that observed in the compression experiments: exfoliation of external sheets of nanoparticles when internal layers of solid lubricant particles are preserved (see Fig. 15). It is clear that the hydrostatic compression model does not reflect all the phenomena occurring in the friction contact. Some peculiarities in the behavior of solid lubricant particles under compression helped us to understand better various effects observed under friction and wear of the IF nanoparticles.

6. Conclusions

1. A phenomenological model describing the constitutive behavior of nanoparticle media during a general isotropic compression has been developed. Hydrostatic powder compression experiments were carried out. Separate low and high density ranges are observed under compression of the solid lubricant media.

2. The compressibility of the IF-WS_2 nanoparticles is much larger than that of both 2H-WS_2 and copper powders under low pressure range. The comparison of the initial yield point Y_S of WS_2 fullerene-like nanoparticles with that of platelet WS_2 and Copper particles show that Y_S of WS_2 is minimal while the hardening coefficient is maximal.

3. A compressibility of IF nanoparticle medium at the high pressure range is lower than that of other powders.

4. Compression with the maximal pressure (500 MPa) showed that the shape of the IF nanoparticles is preserved. The dominant mechanism of damage was found to be the delamination or peeling-off of the external sheets of hollow nanoparticles. Strong destruction of 2H-WS_2 platelets was observed under compression.

5. It was shown that these nanoparticles are capable of withstanding a high hydrostatic pressure, caused by compression without suffering heavy damage.

6. The results obtained in this work allow to understand better the friction and wear behavior of IF-WS_2 nanoparticles in the interface between rubbed surfaces.

Acknowledgement

This work was supported in part by Nanomaterials Ltd.

References

1. L. RAPOPORT, YU BILIK, M. HOMYONFER, S. R. COHEN, and R. TENNE, *Nature* **387** (1997) 791.
2. D. J. SROLOVITZ, S. A. SAFRAN, M. HOMYONFER and R. TENNE, *Phys. Rev. Lett.* **74** (1995) 1778.
3. A. ZAK, Y. FELDMAN, V. ALPEROVICH, R. ROSENTSVEIG and R. TENNE, *J. Am. Chem. Soc.* **122** (2000) 11108. *J. Am. Chem. Soc.* **122** (2000) 11108.
4. J. H. ATKINSON, "An Introduction to the Mechanics of Soils and Foundations: Through Critical State Soil Mechanics" (McGraw-Hill Book Co., London and New York, 1993).
5. SEONG-JUN PARK, HEUNG NAM HAN, KYU HWAN OH and DONG NYUNG LEE, *Int. J. of Mech. Sci.* **41** (1999) 121.
6. T. C. TSZENG and W. T. WU, *Acta Mater.* **44** (1996) 3543.
7. S. BROWN and G. ABOU-CHEDID, *J. Mech. Phys. Solids.* **42** (1994) 383.
8. B. B. HWANG and S. KOBAYASHI, *Int. J. Mach. Manufact.* **30** (1990) 309.
9. N. A. FLECK, L. T. KUHN and R. M. MCMEEKING, *J. Mech. Phys. Solids.* **40** (1992) 1139.
10. S. SHIMA and M. MIMURA, *Int. J. Mech. Sci.* **28** (1986) 53.
11. T. C. TSZENG, W. T. WU, L. FERGUSON and G. PETRUS, in "Net Shape Processing of Powder Materials" (ASME AMD, ASME, New York, 1995) Vol. 216, p. 141.
12. J. BESSON and M. ABOUAF, *Int. J. Solids Struct.* **29** (1991) 691.
13. J. LIAN and S. SHIMA, *Int. J. Num. Meth. Eng.* **37** (1994) 763.
14. D. N. LEE and H. S. KIM, *Powd. Metall.* **35** (1992) 275.
15. J. LANGFORD and D. LOUËR, *Rep. Prog. Phys.* **59** (1996) 131.
16. G. K. WILLIAMSON and W. H. HALL, *Acta Metall.* **1** (1953) 22.
17. "CRC Handbook of Chemistry and Physics" (CRC Press, Inc., 1989).
18. U. S. SCHWARZ, S. KOMURA and S. A. SAFRAN, *Europhys. Letters* **50** (2000) 762.
19. Q. ZHU, T. SEKINE, K.S. BRIGATTI, S. FIRTH, R. TENNE, H.W. KROTTO and D. R. M. WALTON, *J. Am. Chem. Soc.* **125** (2003) 1329.
20. L. RAPOPORT, M. LVOVSKY, I. LAPSKER, V. LESHCHINSKY, YU VOLOVIK, Y. FELDMAN and R. TENNE, *NanoLetters* **1** (2001) 137.
21. L. RAPOPORT, Y. FELDMAN, M. HOMYONFER, H. COHEN, J. SLOAN, J. L. HUTCHISON and R. TENNE, *Wear* **225–229** (1999) 975.
22. L. RAPOPORT, V. LESHCHINSKY, I. LAPSKER, YU. VOLOVIK, O. NEPOMNYASHCHY, M. LVOVSKY, R. POPOVITZ-BIRO, Y. FELDMAN and R. TENNE, *Wear* **255** (2003) 785.

Received 26 August 2003
and accepted 18 March 2004